THE ASTRONOMICAL JOURNAL, 122:1758–1769, 2001 October

H I IN THE SHELL ELLIPTICAL GALAXY NGC 3656[1]

MARC BALCELLS,[2] J. H. VAN GORKOM,[3] RENZO SANCISI,[4,5] AND CARLOS DEL BURGO[2,6]

Received 2001 June 26; accepted 2001 July 10

ABSTRACT

Very Large Array[7] neutral hydrogen observations of the shell elliptical galaxy NGC 3656 reveal an edge-on, warped minor-axis gaseous disk ($M_{\rm H\,I} \sim 2 \times 10^9\ M_\odot$) extending 7 kpc. H I is also found outside the optical image, on two complexes to the northeast and northwest that seem to trace one or two tidal tails, or possibly an outer broken H I disk or ring. These complexes link with the outer edges of the inner disk and appear displaced with respect to the two optical tails in the galaxy. The disk kinematics is strongly lopsided, suggesting recent or ongoing accretion. Integral-field optical fiber spectroscopy at the region of the bright southern shell of NGC 3656 has provided a determination of the stellar velocities of the shell. The shell, at 9 kpc from the center, has traces of H I with velocities bracketing the stellar velocities, providing evidence for a dynamical association of H I and stars at the shell. Within the errors the stars have systemic velocity, suggesting a possible phase-wrapping origin for the shell. We probed a region of $40' \times 40'$ (480 kpc × 480 kpc) × 1160 km s^{-1} down to an H I mass sensitivity (6 σ) of $3 \times 10^7\ M_\odot$ and detect five dwarf galaxies with H I masses ranging from 2×10^8 to $2 \times 10^9\ M_\odot$, all within 180 kpc of NGC 3656 and all within the velocity range (450 km s^{-1}) of the H I of NGC 3656. The dwarfs had been previously cataloged, but none had a known redshift. For the NGC 3656 group to be bound requires a total mass of (3–7.4) $\times 10^{12}\ M_\odot$, yielding a mass-to-light ratio from 125 to 300. The overall H I picture presented by NGC 3656 supports the hypothesis of a disk-disk merger origin or possibly an ongoing process of multiple mergers with nearby dwarfs.

Key words: galaxies: elliptical and lenticular, cD — galaxies: general — galaxies: interactions — galaxies: kinematics and dynamics — galaxies: peculiar

1. INTRODUCTION

NGC 3656 (Arp 155) is a peculiar elliptical galaxy with a nearly spherical body and a dark band running north-south (see Fig. 1). A light clump can be seen 45″ south of the center, which is bound to the south by a prominent shell. A number of other, nearly circular shells are seen around the galaxy. The core rotation axis is orthogonal to that of the main body (Balcells & Stanford 1990, hereafter BS90). Two faint optical tails exist around the galaxy (Balcells 1997, hereafter B97). Color maps of the galaxy (B97) show that the shell to the south is distinctly blue ($B-R \approx 0.95$) in relation to the surroundings ($B-R \approx 1.4$), pointing to a young age for its stars. Star formation ($\sim 0.1\ M_\odot$ yr^{-1}) is ongoing at the dust lane, as evidenced by extended emission in Hα (B97) and radio continuum (Möllenhoff, Hummel, & Bender 1992).

Observations of the 21 cm hydrogen emission line obtained with the Westerbork Synthesis Radio Telescope (WSRT) show that the galaxy contains about $10^9\ M_\odot$ of neutral hydrogen (Balcells & Sancisi 1996, hereafter BS96). The H I distribution peaks on the dust lane and extends in the north-south direction. The gas on the dust lane shows rapidly rising rotation with velocities reaching up to about 225 km s^{-1}, supporting the hypothesis of a rotating disk seen almost edge-on. In addition to this H I component, there is a central concentration of molecular gas of similar mass (BS96).

NGC 3656 is useful for the study of the origin of gaseous disks in elliptical galaxies because of the large number of peculiarities normally ascribed to interactions that coincide in this galaxy: shells, two tails, peculiar kinematics, peculiar colors, and star formation. These can provide constraints on formation scenarios for the gaseous disk. In addition, NGC 3656 is interesting for the study of the H I–shell relation, because of the apparently young dynamical age of the system and because the southern shell is significantly brighter (1.5 mag arcsec^{-2}) than the galaxy background at that distance from the center.

We present here Very Large Array (VLA) aperture synthesis H I observations and integral-field spectroscopy (IFS) using fiber optics on NGC 3656. H I measurements are used to describe the gas distribution and velocities with higher resolution and sensitivity than achieved with the WSRT and to look for the existence of diffuse gas around the galaxy. The IFS of the shell to the south has provided an optical velocity determination for stars associated with the shell.

The optical IFS is presented in § 2. Section 3 describes the H I observations. Results are presented in § 4, for the inner H I disk (§ 4.1), for the extended H I (§ 4.2), and for the shell kinematics (§ 4.3). We discuss the H I results in § 5, the connection between H I and the shell in § 5.1 and possible formation scenarios for NGC 3656 in § 5.3. A Hubble constant of 75 km s^{-1} Mpc^{-1} and a distance of 40 Mpc are

[1] Based on observations made with the William Herschel Telescope operated on the island of La Palma by the Isaac Newton Group of Telescopes in the Spanish Observatorio del Roque de los Muchachos of the Instituto de Astrofísica de Canarias.

[2] Instituto de Astrofísica de Canarias, C/ Vía Láctea, 38200 La Laguna, Canary Islands, Spain.

[3] Department of Astronomy, Columbia University, 550 West 120th Street, New York, NY 10027.

[4] Osservatorio Astronomico di Bologna, Via Ranzani 1, I-40127, Italy.

[5] Kapteyn Astronomical Institute, University of Groningen, Postbus 800, 9700 AV Groningen, Netherlands.

[6] Max Planck Institut für Astronomie, Königstuhl 17, D-69117 Heidelberg, Germany.

[7] The Very Large Array of the National Radio Astronomy Observatory is operated by Associated Universities, Inc., under cooperative agreement with the National Science Foundation.

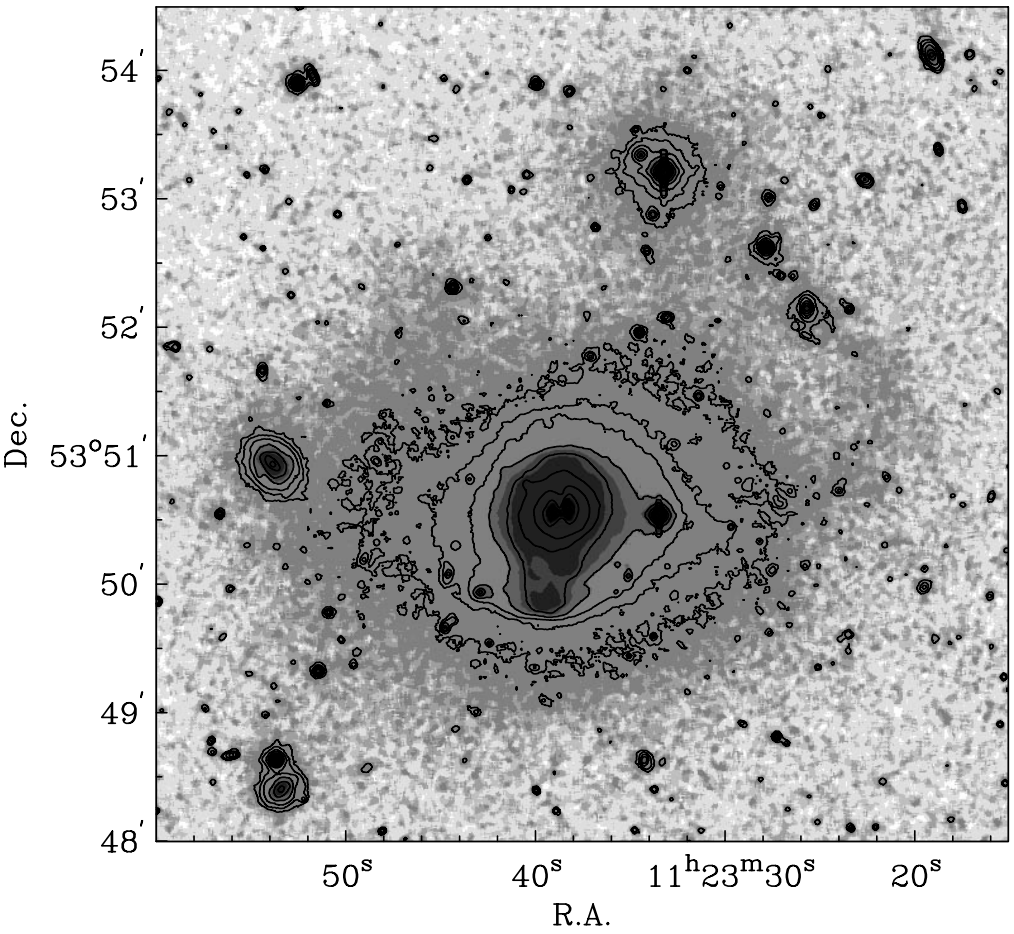

FIG. 1.—*R*-band image of NGC 3656 (from Fig. 1 of B97). Lowest contour is 26.0 mag arcsec^{-2}, contour spacing is 0.75 mag. Gray levels, drawn after applying a 5 pixel × 5 pixel median filter, correspond to sky $-3\,\sigma$ (*white*), sky $-2\,\sigma$, sky $-\sigma$, sky $+\sigma$, sky $+2\,\sigma$, and sky $+3\,\sigma$ to show the faintest extended optical structures. Flat-fielding of the image is better than 0.2%. Objects at (α, δ) = ($11^h23^m33^s$, 53°50′33″), ($11^h23^m33^s.1$, 53°53′13″), and ($11^h23^m27^s.7$, 53°52″38″) are stars. Scale is 0.2 kpc arcsec^{-1}.

assumed throughout, giving a scale of 0.2 kpc arcsec^{-1}. All coordinates refer to the J2000.0 equinox.

2. INTEGRAL-FIELD OPTICAL FIBER SPECTROSCOPY

We observed the southern shell of NGC 3656 with the William Herschel Telescope on 1998 March 31, using the INTEGRAL fiber bundle system that feeds the WYFFOS Nasmyth spectrograph. For a description of INTEGRAL, see Arribas et al. (1998). We used the SB3 bundle, which contains 135 fibers, each 600 μm in diameter (2″.7 on the sky). Of these, 115 densely cover an area of 34″ × 30″ on the sky. The distribution of these fibers is hexagonal with a mean distance between them of 3″. The remaining 20 fibers are set in a ring 45″ in diameter, which is generally used for a sky measurement. We used grating R1200R, which gives a mean dispersion of 1.4 Å pixel^{-1} in the spectral range 5640–7070 Å (covering the Na I doublet at 5890 Å, the λ6563 Hα line, and the [S II] $\lambda\lambda$6716 and 6731 lines). The optical fiber bundle was positioned at (α, δ) = ($11^h23^m38^s.6$, 53°49′57″.6), ~35″ south of the galaxy center, and covers from the southern end of the dust lane to beyond the southern end of the shell. The region covered by the bundle is indicated with a thick rectangle in Figure 5.

We followed the data reduction procedure described in del Burgo (2000): bias subtraction, aperture definition and trace, stray light subtraction, extraction of the apertures, wavelength calibration, throughput correction, sky subtraction, and cosmic-ray rejection. The throughput correction was done from sky and dome flat exposures. Sky subtraction was accurate to better than 5% rms.

The individual spectra show the Na I absorption doublet and traces of Hα, N II, and S II emission lines. The weakness of these lines indicates a very slow rate of star formation activity in the shell at present. However, Hα absorption indicates that star formation must have been important in the past $\sim 10^9$ yr. Overall, the distribution of the Hα emission matches the one displayed in the Hα narrowband image in Figure 2*b* of B97.

We obtained stellar velocities via cross-correlation, using the spectrum of a G2 V star as a template. We opted not to use the Hα line because, in many fibers, this is partially filled with Hα emission. Instead, we used the region around 5890 Å, which includes the Na I doublet. We cross-correlated each fiber spectrum and excluded those where no convergence was found. We then co-added groups of spectra that showed similar velocities and cross-correlated these with the template to verify that the results do not depend on the signal-to-noise ratio of the spectra. Because of the intrinsic low signal of each spectrum, the individual fiber velocities have errors around 100 km s^{-1}. Co-added spectra yield velocities with errors around 60 km s^{-1}. The errors are probably conservative since cross-correlation is known

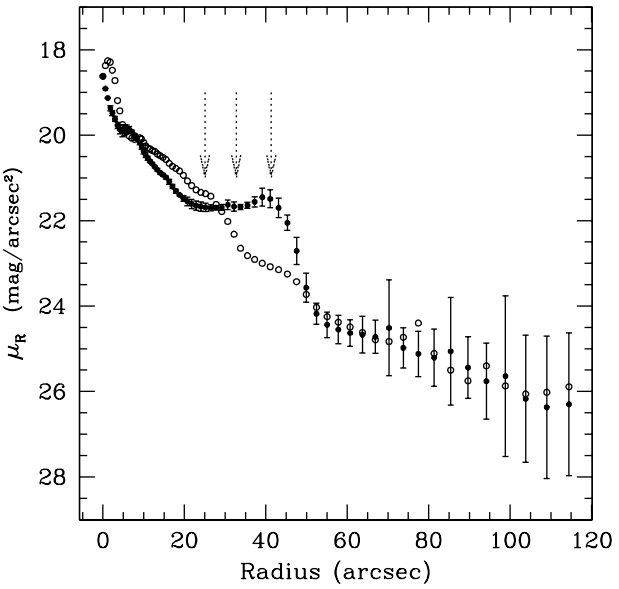

FIG. 2.—*R*-band surface brightness profiles of NGC 3656 on 25°-wide wedge-shaped apertures centered on the galaxy nucleus, along P.A. = 170° (*filled symbols, with error bars*) and along P.A. = 10° (*open symbols, error bars omitted*). Vertical arrows indicate the central positions of the apertures where optical velocities from two-dimensional fiber spectroscopy are measured.

to overestimate velocity errors (BS90; Jedrzejewski & Schechter 1988). This yielded three velocity values centered at positions 25″, 33″, and 41″ south of the center. These synthesized apertures are indicated with rectangles in Figure 5.

To show the three optical velocity apertures with respect to the southern shell, we plot *R*-band surface brightness profiles along wedge-shaped apertures along P.A. = 170° and P.A. = 10°, centered on the galaxy nucleus (Fig. 2). The vertical arrows locate the center positions of the three fiber velocity data apertures. We take the north profile as an estimate of the underlying galaxian surface brightness distribution and use this to measure the surface brightness contrast at the southern shell. The latter, at $R = 45''$, has $\mu_R = 21.5$ mag arcsec^{-2}, 1.5 mag arcsec^{-2} brighter than the background. The outermost velocity point is centered on the southern shell; thus, the measurement traces the shell velocity with little background contamination. At the locations of the two innermost measurements, the north and south surface brightnesses are comparable, suggesting that these two measurements trace the underlying galaxy velocity field. Optical velocity results are presented in § 4.3.

3. H I OBSERVATIONS

Neutral hydrogen VLA observations were made in D array (1 km) in 1996 September. The VLA data confirmed the presence of H I associated with the dust lane and southern shell inferred in the WSRT data and also revealed the presence of low surface brightness extended H I around the galaxy. The H I emission at anomalous velocities in the southern shell region (Fig. 2 of BS96) was not confirmed. The data looked complex enough for a proper multiconfiguration study to allow the gas to be compared with optical structures on all scales. Here we present the combined results of 4 hr of D, 8 hr of C, and 16 hr of B configuration data taken in 1996 September, 1997 September, and 1997 February, respectively. For all observations, a total bandwidth of 6.25 MHz was used, centered at 2870 km s^{-1}. The correlator was used in 2 IF mode with no on-line Hanning smoothing. This produced 63 channels, with 21 km s^{-1} channel separation. Usable data were obtained over the velocity range from 2365 to 3521 km s^{-1}. Standard VLA calibration procedures were used; initially separate data cubes were made for each of the configurations to inspect the data. Then the continuum was subtracted in the UV plane by making a linear fit through the line-free channels. The UV data were then combined, and image cubes were made with various weighting schemes. Here we present the results of the full-resolution data, using uniform weight and robust 1, giving an angular resolution of 7.″3 × 7.″2 and an rms noise of 0.16 mJy beam^{-1} (1 mJy beam^{-1} = 11.4 K), and images made of the C and D array only, with a resolution of 25.″2 × 19.″7 and an rms noise of 0.23 mJy beam^{-1} (1 mJy beam^{-1} = 1.21 K). This translates into typical column density sensitivities (2 σ) of 1.4×10^{20} cm^{-2} in the BCD array and 2×10^{19} cm^{-2} in the CD array. Our 6 σ H I mass limit over 40 km s^{-1} is $2 \times 10^7 M_\odot$ in the center of the field.

4. RESULTS

H I associated with NGC 3656 is detected over the range of 2600–3100 km s^{-1}, with an integrated H I flux of 5.4 ± 0.4 Jy km s^{-1}, in good agreement with the single-dish value of 5.3 ± 1 Jy km s^{-1} obtained at Jodrell Bank (BS96). In addition, five small spiral and dwarf irregular galaxies are detected within the velocity range of NGC 3656, all within ~180 kpc of NGC 3656. Figure 3 shows the total H I distributions for the six detected galaxies over a Digitized Sky Survey (DSS) image. None of the companions had a previously measured redshift. The parameters of these galaxies are listed in Table 1. Together, the observations indicate that NGC 3656 is in an H I–rich environment.

MGC +09-19-059, at 24 kpc to the southwest of NGC 3656, shows an outer H I extension toward the south. At very low levels (1 σ), there is evidence for a bridge between MCG +09-19-056 and MCG +09-19-059 at 2744 km s^{-1}, and at even lower levels there may be a connection between MCG +09-19-059 and NGC 3656 at 2807 km s^{-1}.

The H I density distribution of NGC 3656 shows a north-south disk seen almost edge-on, which coincides in the inner part with the dust band, and extensions on a larger scale surrounding the optical picture. At the galaxy center, there is a radio continuum source slightly extended north-south and coinciding with the dust lane. It has a peak of 10 mJy beam^{-1} and total flux density of 24 ± 1 mJy. This source had been reported by Möllenhoff et al. (1992).

4.1. *The Inner* H I *Disk*

The distribution and kinematics of the gas at the highest angular resolution of 7″ is displayed in the channel maps of Figure 4. The high-resolution total H I map (Fig. 5) shows a concentration of H I running north-south in the inner parts and well aligned with the dust lane. This forms an inner disk seen nearly edge-on. The central, innermost contour encircles a local minimum due to absorption against the central radio continuum source. Further out, the disk seems to become warped, oriented more northwest-southeast and apparently more face-on. The kinematic structure of the edge-on disk is shown in the position-velocity map at position angle 170° (Fig. 6). This is in the direction from the

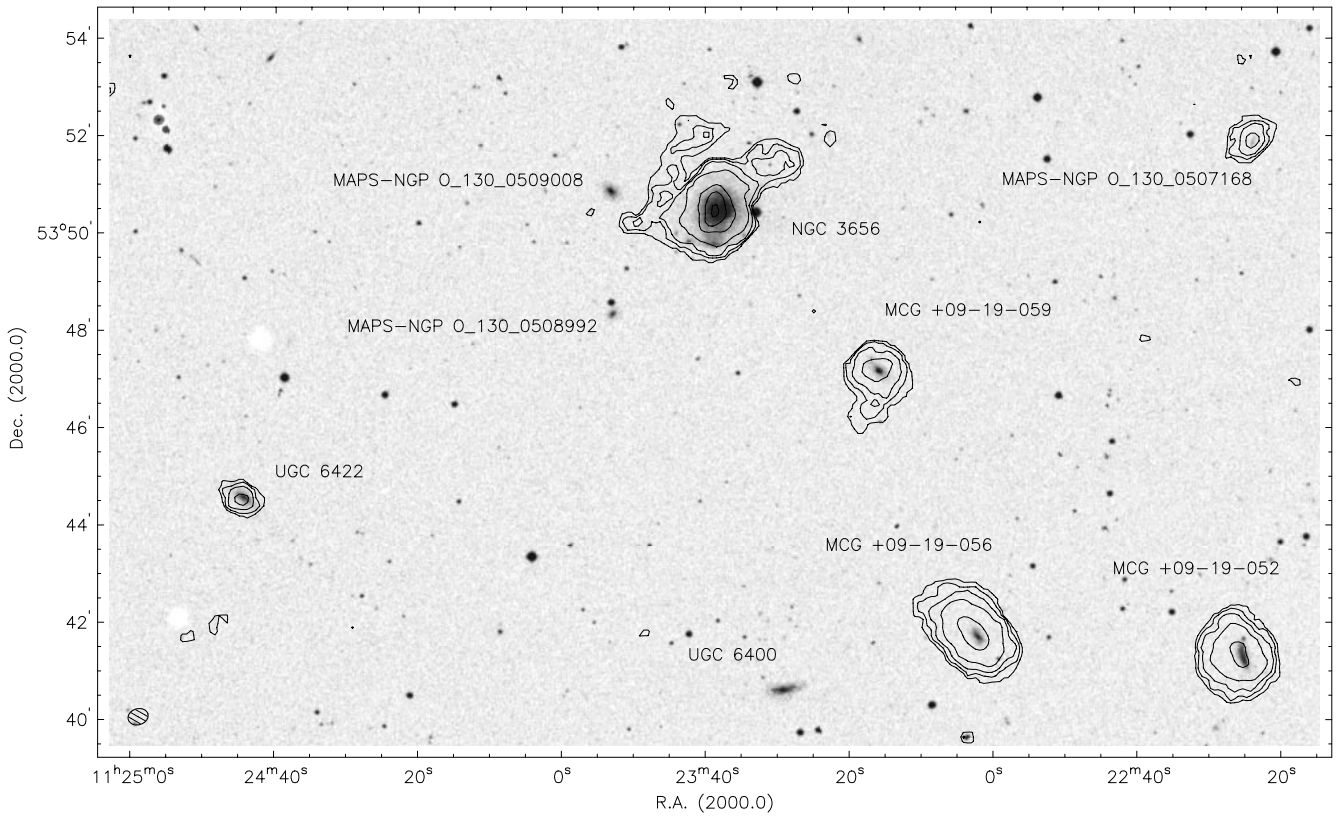

FIG. 3.—Total H I contours from the C and D array data (25″ resolution) overlaid on a DSS image. Field size is 25′ × 15′. H I contours are 0.23, 0.57, 1.1, 2.3, 6.8, 11.4, and 16.0 × 10^{20} cm^{-2}.

center to the southern optical shell. The pattern of rotation is clear, with the southern side receding and the northern approaching and a steep rise in the rotation curve near the center. The velocity range is from about 2650 to 3100 km s^{-1}, corresponding to 225 km s^{-1} maximum rotational velocity, and the midpoint velocity is approximately 2875 km s^{-1}, in good agreement with the optically determined stellar systemic velocity (2869 ± 13 km s^{-1}; BS89). The warped disk extends to 35″ (7 kpc) from the center.

The disk kinematics is strongly lopsided. While inside 10″ of the center, where the maximum rotational velocity of 225 km s^{-1} is reached, the rotation pattern is symmetric, beyond 10″ the rotational velocities remain constant on the northern side whereas they drop by a factor of 2 (∼100 km s^{-1}) on the southern side. This asymmetric velocity structure indicates large deviations from circular motion—possibly gas on eccentric orbits suggesting a young dynamical age for the disk. Noncircular motions may contribute to the important velocity broadening toward systemic velocity visible on both sides of the galaxy. On the southern side, low-velocity gas (2912 km s^{-1}, 35 km s^{-1} above systemic) is seen at all radii. There are traces of emission at apparently counterrotating velocities, approaching in the southern (2800 km s^{-1}) and receding in the northern quadrant. These may partly be explained by the outer warp geometry. They may also trace H I in highly elongated orbits associated with the southern shell (see § 4.3).

The effect of absorption against the central radio continuum source is clearly shown by the hole near the systemic velocity in the position-velocity map (Fig. 6), as expected in

TABLE 1

H I DATA FOR NGC 3656 AND DETECTED COMPANIONS

NAME	R.A. (2000)	DECL. (2000)	$V_{H I}$ km s^{-1}	$\Delta(V_{H I})$[a] km s^{-1}	$M_{H I}$[b] Jy km s^{-1}	$M_{H I}$[b] 10^9 $M_\odot$
NGC 3656	11 23 38.4	53 50 30	2870	425	5.40	2.0
MAPS-NGP O130-0507168.....	11 22 23.6	53 51 54	3059	105	0.47	0.18
MCG +09-19-052	11 22 25.2	53 41 17	2944	168	3.40	1.3
MCG +09-19-056	11 23 02.5	53 41 47	2796	168	4.99	1.9
MCG +09-19-059	11 23 16.0	53 47 14	2796	126	0.78	0.29
UGC 6422	11 24 44.7	53 44 36	2996	126	0.45	0.17

NOTE.—Units of right ascension are hours, minutes, and seconds, and units of declination are degrees, arcminutes, and arcseconds.

[a] Full velocity range over which H I is detected.

[b] H I mass uncertainties are approximately 10%.

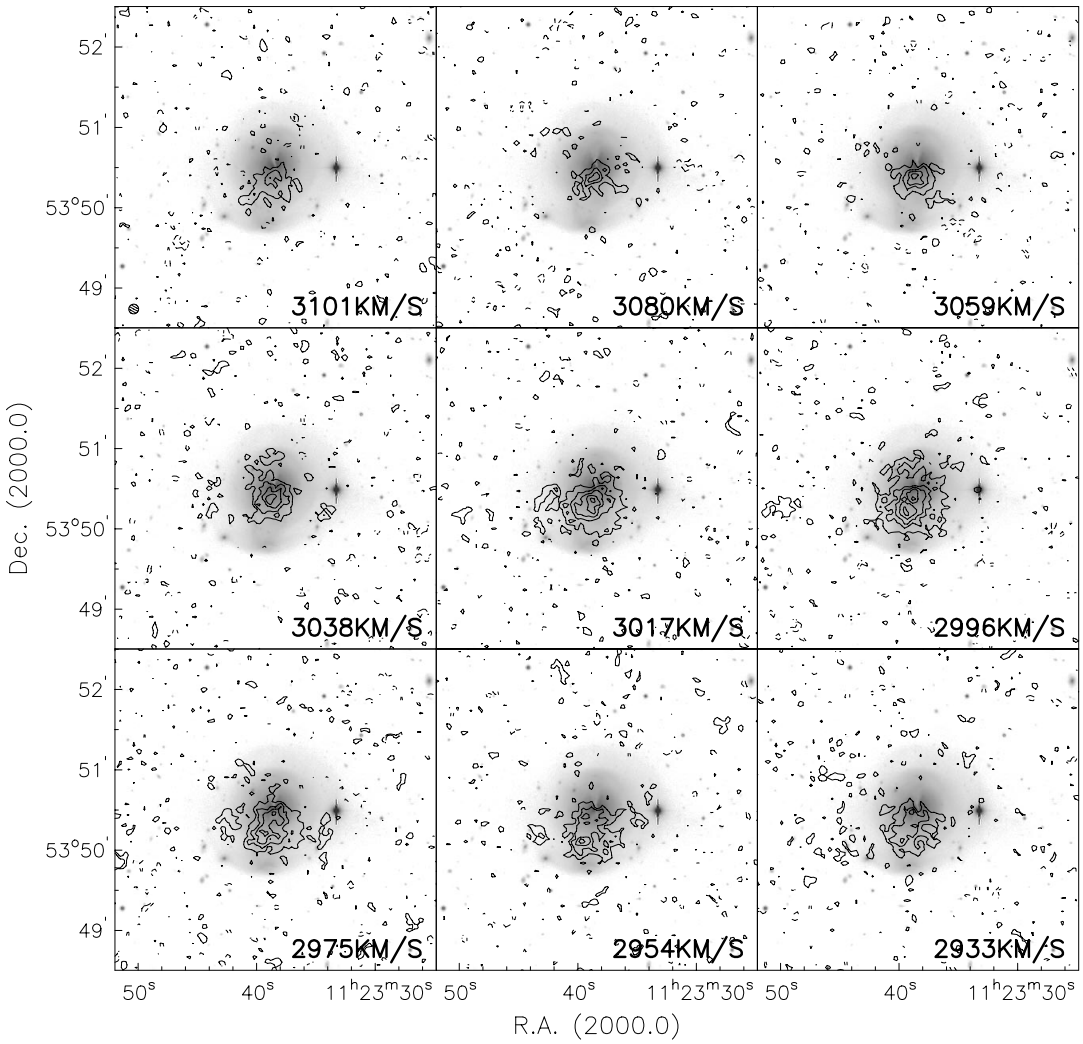

FIG. 4.—Channel maps for the data cube derived from BCD array data. Gray scale is the *R*-band image. Contours are -0.64, -0.32 (*dashed*), 0.32, 0.64, 0.96, 1.128, and 1.60 mJy beam^{-1}. Beam is $7''.3 \times 7''.2$. Noise is 0.16 mJy beam^{-1} rms.

an edge-on disk. The absorption is also present at velocities higher than the systemic velocity (-0.74 mJy at 2891 km s^{-1} and -0.45 mJy at 2870 km s^{-1}). This provides evidence for noncircular motions.

To investigate the relation of the H I and the shell, we plot in Figure 7 a renzogram (Schiminovich, van Gorkom, & van der Hulst 2001): one contour (0.64 mJy beam^{-1}, 3 σ) from each channel map, with color-coded velocity, is plotted on top of a gray-scale *R*-band image. This figure may be used to analyze the relation between the rotating system of H I and the southern shell. H I is detected at the shell in the 2912 km s^{-1} channel only. The channel maps in Figure 4 also show that the H I reaches only the shell in this channel, at the 4 σ level, with traces of H I beyond the shell in the 2870 km s^{-1} channel. The other velocity channels do not quite reach the shell at the 3 σ level. Most velocity contours pile up at $\sim 35''$ from the center. Therefore, despite its proximity, the shell does not appear to lie within the main H I rotating system but is slightly offset to the outside of it. We find measurable H I on the shell, which does not rotate with the main H I disk but, rather, displays a narrow range of near-systemic velocities.

The strong velocity broadening in the disk is apparent in the superposition of the velocity contours, as is the warp geometry. The color coding shows that the intermediate velocities at the northern and southern tips of the disk link smoothly with the extended H I emission further out.

4.2. *Extended Emission*

The C and D array data reveal H I emission further out than the $\sim 35''$ radius of the main disk. The most striking characteristic of the extended emission is its strongly asymmetric distribution with respect to the optical galaxy. The total H I $25''$ resolution map is shown in Figure 8, overlaid on a high-contrast optical image. While on the southern side the H I distribution ends rather sharply at the radius of the main disk, two H I complexes extend to the north. One starts at the southeastern side of the inner H I system and extends like a long arm ($130'' = 26$ kpc) toward the north. Its velocity (Fig. 4) declines smoothly from about 2933 km s^{-1} in the east to 2891 km s^{-1} in its northern tip. Another feature starts at the north end of the inner disk and extends in the northwest direction. Its velocity increases from 2723 km s^{-1} at its base to 2807 km s^{-1} at its tip. These two complexes may be tidal tails, given the asymmetry to the north of the extended distribution and the smooth velocity profiles along the features. An alternative possibility is that they may form part of an outlying, broken, extended, and

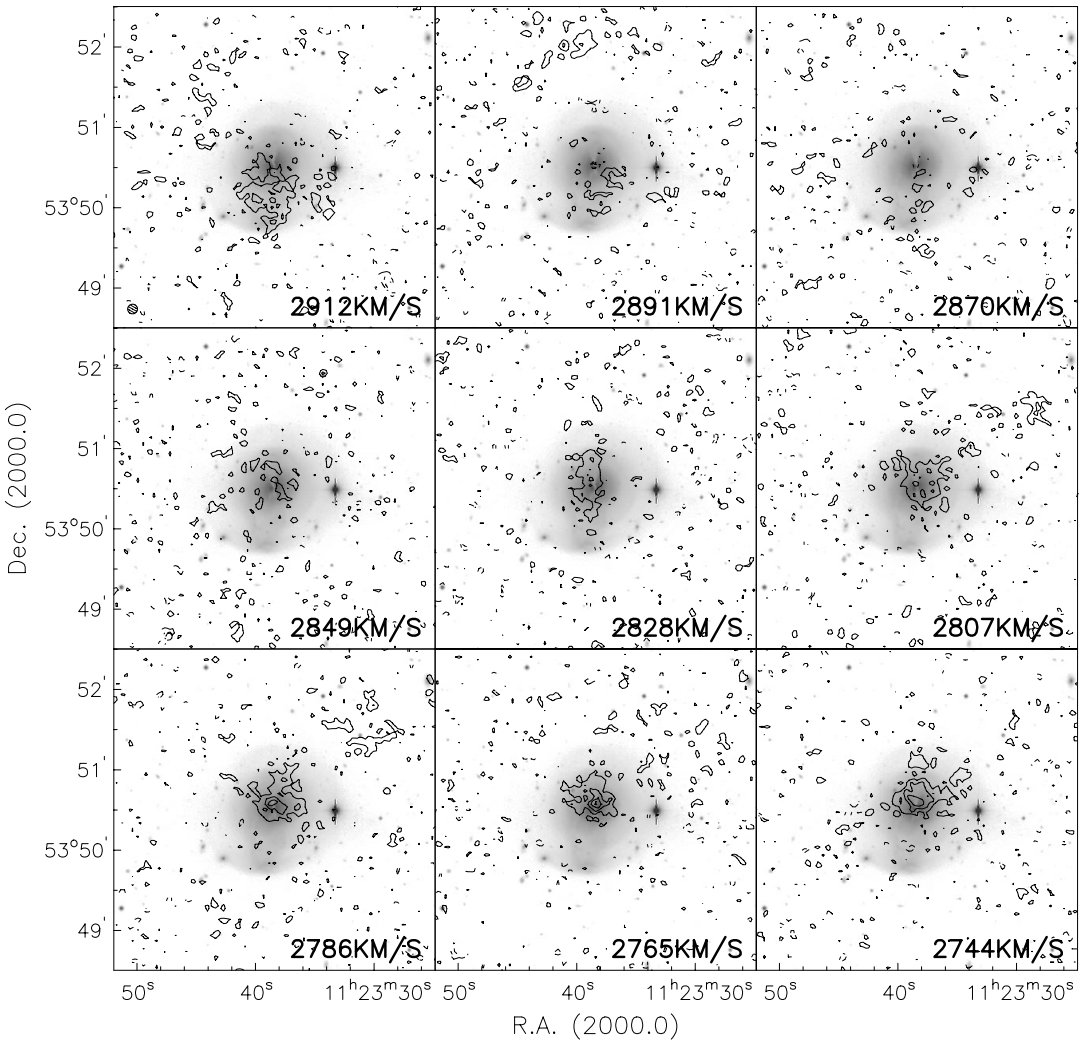

FIG. 4.—*Continued*

warped disk or ring. The observed velocities may then be understood as due to the more face-on view of the outer gas as well as to noncircular motions. These features connect with the warped gaseous disk in the main body of the galaxy. The total H I mass of these two complexes is $1.9 \times 10^8\ M_\odot$, roughly 9% of the total H I detected in the system. The eastern H I feature is parallel but slightly offset inward with respect to the eastern optical tail reported by B97, which is shown in Figure 8. The northwest H I feature has no apparent optical counterpart; the western optical tail curves around the H I (Fig. 8). Such anticorrelation of H I and optical tails has been found in other merger remnants, e.g., NGC 520 (Hibbard & van Gorkom 1996) and NGC 2865 (Schiminovich et al. 1995). See Hibbard, Vacca, & Yun (2000) and Mihos (2001) for possible explanations of these morphologies.

4.3. *Shell Kinematics*

Stellar velocities derived from the integral-field optical fiber spectroscopy (§ 2) are shown in Figure 6 overplotted on the H I position-velocity diagram. The two innermost points lie within the rotating system described in § 4.1, and their velocities match those of the H I. These measurements trace the general stellar velocity field rather than the clump/shell velocity (§ 2). Thus, stars near the galaxy's minor axis rotate with the H I. The stars could have been accreted with the H I or may have formed in place out of the H I disk. The pronounced blue colors in this region ($B-R \sim 0.9$; B97) and the traces of Hα absorption (§ 2) indicate a young age, and the disk is actively forming stars further in, out to 3 kpc from the center (BS96).

At the outermost point the mean velocity is 2886 ± 61 km s^{-1}. This point is centered on the bright clump (see Fig. 2) and thus provides velocity information closest to the southern shell. It is interesting that the velocity at this point lies quite close to the galaxian systemic velocity (2869 ± 13 km s^{-1}). The error bar of the shell velocity, which gives the rms scatter of the individual fiber velocities, constraints the line-of-sight velocity to less than 30% of the galaxy circular velocity, which from the overall H I rotation curve we estimate as $V_{\rm circ} \approx 200$ km s^{-1} at the galactocentric distance of the shell. Even accounting for a comparable velocity component perpendicular to the line of sight, the orbits must be fairly elongated. Trial N-body experiments indicate that, if the shell material is at apocenter with tangential velocity below 30% of the circular velocity, the orbit eccentricity is above 0.8 and the pericenter distance is below $0.3R_{\rm eff}$. Such radial orbit for the clump suggests that the shell results from the piling up of stars at the apocenters of their orbits rather than from the bending of a sheet of stars in near-circular

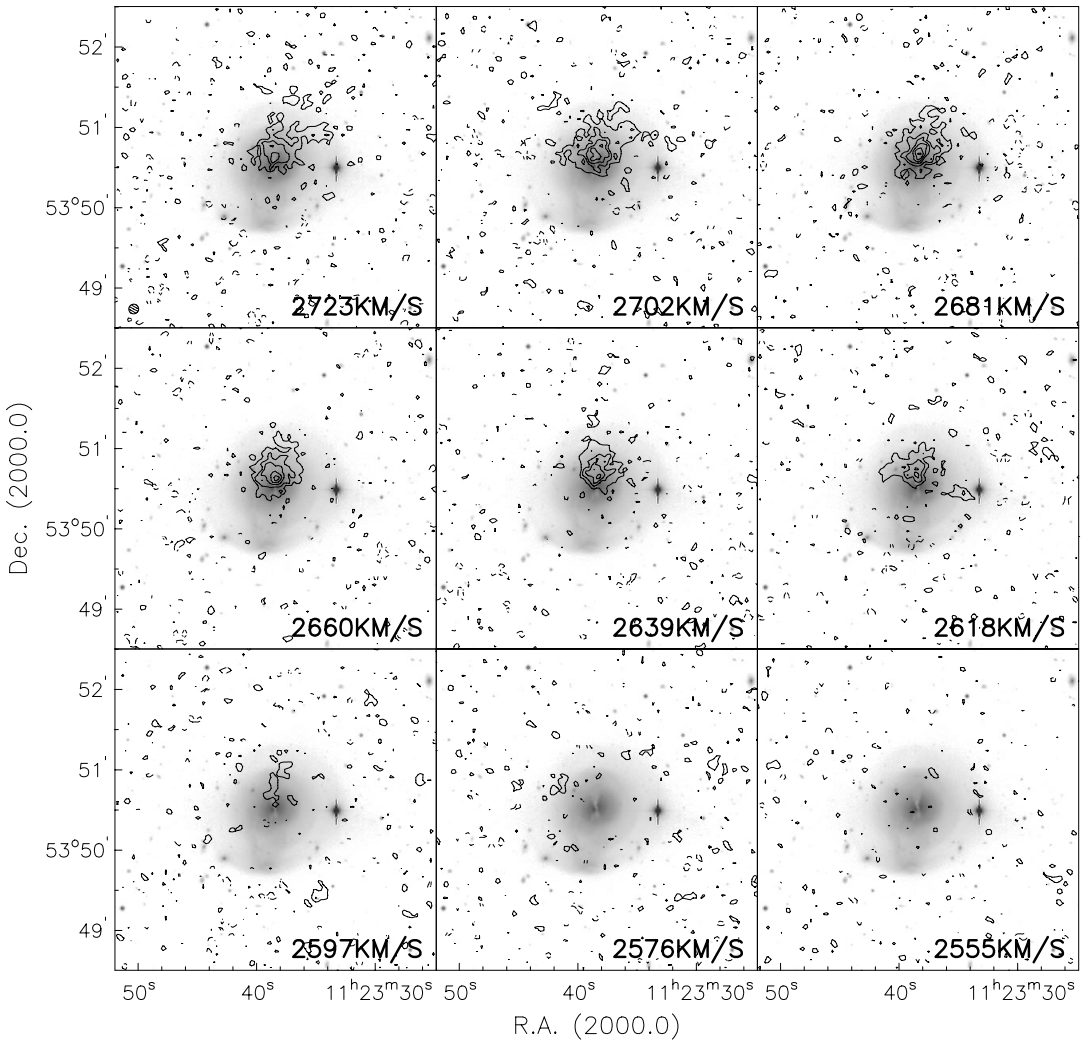

FIG. 4.—*Continued*

orbit seen edge-on at its tangential point. That is, while the stars cannot be constrained to a strictly radial orbit, the shell appears to be more a result of phase wrapping (Quinn 1984) than space wrapping (Dupraz & Combes 1987; Hernquist & Quinn 1987).

At the location of the clump in the shell, H I is detected at 2912 km s^{-1}, plus traces further out than the shell at 2870 km s^{-1} (Figs. 4 and 7). These velocities bracket the optical velocity of the shell. The strong detection at 2912 km s^{-1} (above 4 σ) indicates that the H I at the shell is dominantly at velocities that match the shell stellar velocity and provides kinematic evidence that the H I and the stars are dynamically associated at the shell.

5. DISCUSSION

The elliptical galaxy NGC 3656 has remarkable optical and H I properties. The optical picture is already complex, with a minor-axis dust disk harboring an extended starburst, a north-south blue ring, two optical tails, a prominent shell, and a number of other faint shells (BS90; B97). The H I data presented here adds to the complexity, showing a minor-axis warped gaseous disk and two gaseous complexes or tails extending to the north of the galaxy. The H I distribution is asymmetric in two respects: there is a strong positional asymmetry in the external gas and a strong kinematic asymmetry in the H I disk inside the galaxy. Neutral hydrogen appears to be dynamically associated with the shell to the south of the main body.

Main questions on the H I disk structure are the pronounced broadening of the position-velocity distribution toward systemic velocity and the strong velocity lopsidedness (Fig. 6). Modeling will be needed to determine the relative importance of the warp, the disk internal velocity dispersion, and line-of-sight integration effects on the velocity broadening. Modeling may clarify as well if elliptical orbits in the disk or associated with the shell are required to explain the velocity lopsidedness.

It is likely that the asymmetry in the H I velocity distribution is also related to accretion from the external complexes, with H I dominantly falling from the north causing the observed kinematic asymmetries. That accretion is taking place may be inferred from the geometry of the east complex: for this system to wrap around the galaxy, from its base on the south to its north tip, it needs to be on the near side to the observer; otherwise, its angular momentum would be opposite to that of the gas disk. The velocities above systemic, then, indicate that the gas in the complex is falling onto the galaxy.

An order-of-magnitude estimate of the gas accretion rate may be derived from the masses and velocities of the exter-

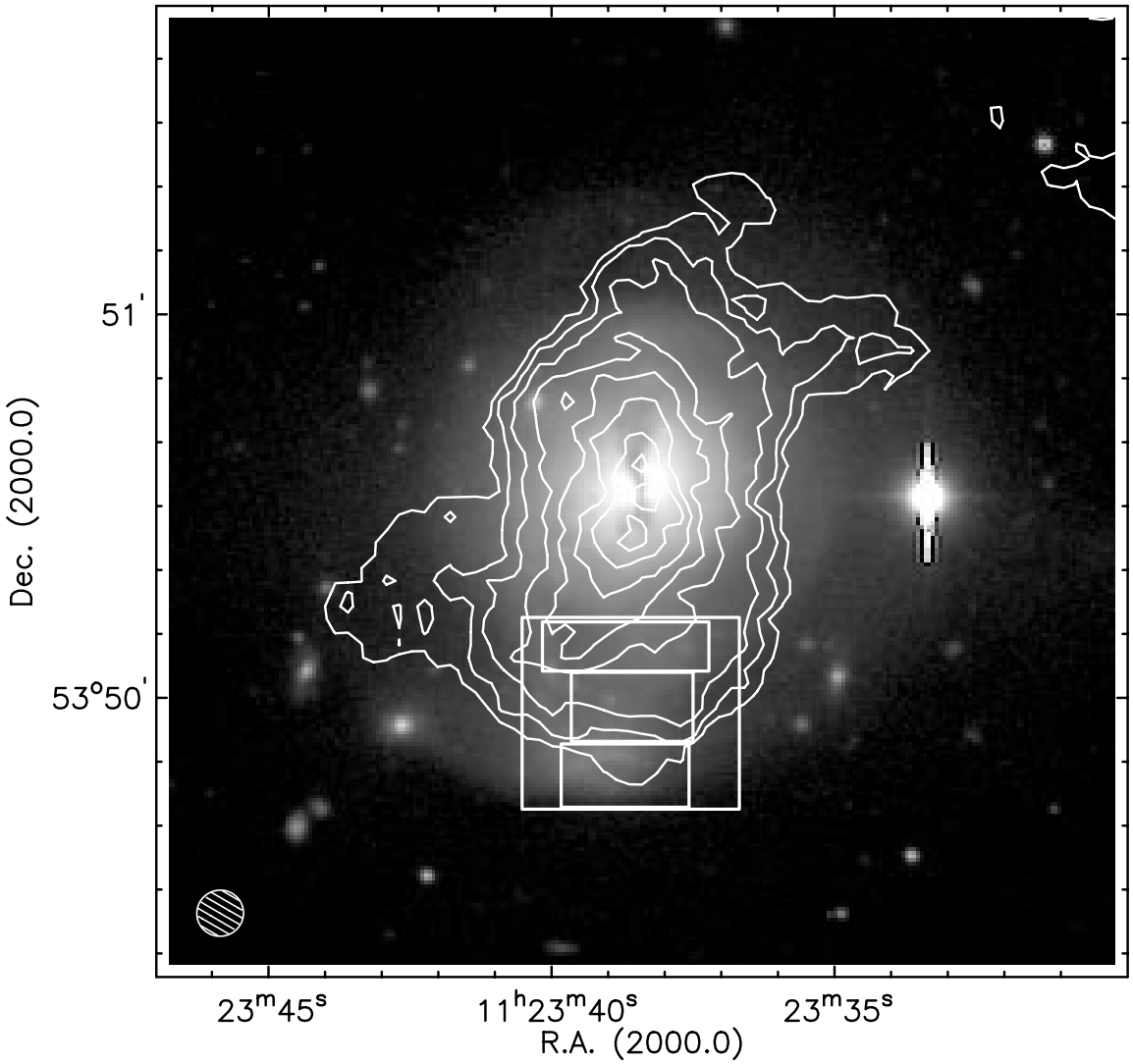

FIG. 5.—Contours of total H I flux from BCD array data. Beam is 7″ FWHM. H I contours are 2.1, 5.2, 10, 21, 31, 42, 52, and 62 × 10^{20} cm^{-2}. *Thick box:* Aperture of the two-dimensional fiber bundle spectrograph. *Thin boxes:* Synthetic apertures for stellar velocities derived from the two-dimensional optical fiber spectroscopy.

nal complexes. For the northeast arm, the rate is $\sim 0.2\ M_{\odot}$ yr^{-1}. At this rate, both systems would take 5 Gyr to deliver the gas currently present inside NGC 3656. Accretion is likely to have been more efficient in the past; hence, the age of the event that originated the accretion is likely to be much shorter. If the rate continues as it is now, NGC 3656 will continue to accrete gas for at least another ~ 0.5 Gyr, probably longer if the tips of the arms are on less bound orbits.

That the external complexes trace tidal tails rather than an external disk or ring remains open to interpretation, as is the case for the extended H I distributions in other merger remnants (NGC 520, Hibbard & van Gorkom 1996; NGC 5128, Schiminovich et al. 1994). Tails and inclined rings may have similar kinematic signatures when seen in projection, despite tails being on fairly elongated orbits. In NGC 3656, the strong lopsidedness of the external H I together with the kinematic peculiarities in the inner disk favor the tail interpretation. But it is unclear whether the extended material, or part of it, describes an extension of the inner warped disk. In either interpretation, the long dynamical times in the outer parts make it unclear what the evolution of the gas and stars might be when the merger signatures in the inner parts fade out. Some of this material may evolve into the type of H I–delineated outer shells seen in, e.g., NGC 5128 and NGC 2865 (Schiminovich et al. 1994, 1995)—see in particular the channel maps at 2912 and 2891 km s^{-1}.

As the system evolves, the disk should grow in radius as the high angular momentum material at high radii settles into organized orbits. This should happen in about 1 Gyr, roughly the orbital period at the tip of the extended complexes at 26 kpc.

5.1. *Shell Dynamics*

The first detection of H I near the shells in NGC 5128 (Schiminovich et al. 1994) brought the question of whether gas and shell stars are dynamically associated or simply projected along the line of sight (van Gorkom & Schiminovich 1997). Our measurements provide evidence that the shell stars and the H I in NGC 3656 share a similar line-of-sight velocity and hence are most likely dynamically associated.

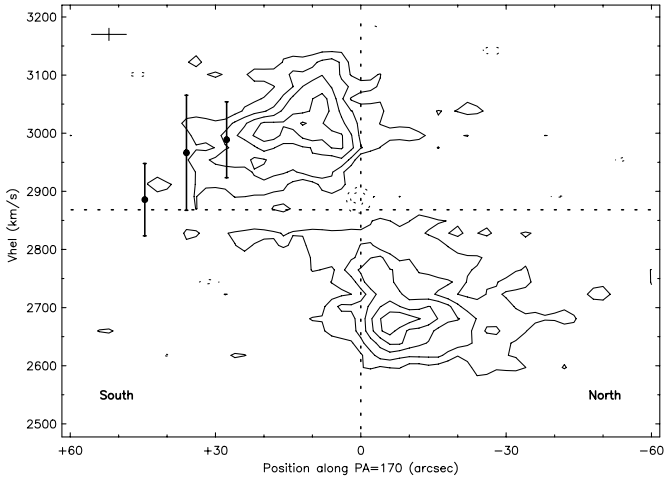

FIG. 6.—*Contours:* Position-velocity diagram along position angle 170°, centered on the nucleus of NGC 3656. The origin is set at the position of the radio continuum source. The horizontal dotted line indicates the optically determined systemic velocity (2969 km s^{-1}). The cross indicates the spatial resolution (7″) and velocity resolution (21 km s^{-1}). Contours are −0.96, −0.64, −0.32 (*dotted*), 0.32 (2 σ), 0.64, 0.96, 1.128, and 1.60 mJy $beam^{-1}$. *Points:* Na I λ5890 optical stellar velocities derived from two-dimensional optical fiber spectroscopy near the southern shell. Note the absorption at slightly redshifted velocity.

To our knowledge the southern shell in NGC 3656 is the first shell for which stellar velocity information becomes available. Our results show that IFS provides a means for obtaining velocity information of shells and other extended, low surface brightness objects by co-adding over two-dimensional apertures. Our formal errors are large, highlighting the difficulty of the measurement, and deeper data will be valuable to confirm the results. We attempted this measurement on NGC 3656 because the southern shell is significantly brighter than most shells in other galaxies. However, in NGC 3656 the measurement is made difficult by weak line strengths due to low metallicity and/or dilution by a young stellar continuum throughout this galaxy (see the spectrophotometric data on NGC 3656 in Liu & Kennicutt 1995). IFS measurements of shell stellar kinematics may be successful on massive ellipticals with red shells, even if fainter than the shell observed here.

Our measurement highlights the possibility to sort out the phase-wrapping versus space-wrapping dichotomy for shells on the basis of data. To date, dynamical models for shells have had to rely on morphological information only to constrain the types of orbits of the shell material.

It was unexpected to us that the NGC 3656 shell should be on a phase-wrapping orbit. There is little evidence for shell interleaving in this type 2 (Prieur 1990) shell system. Given the shell's proximity to the disk of H I, we suspected a low- to moderate-ellipticity orbit for the shell material, hence a space-wrapping nature for the shell. In the similar galaxy NGC 5128, the high angular momentum of the stellar halo traced by planetary nebulae (Hui et al. 1995) and the high rotation velocity of the H I near the shells together point to high-angular momentum shells (Schiminovich et al. 1995). To explain the nearly radial orbit of the shell of NGC 3656, one possibility is that disruption near pericenter and dynamical friction remove angular momentum from the collisionless component of the merging object, so that stars and gas decouple from each other. Gas and stars should be expected to follow different dynamics during the merger anyway for the gas to form an ordered disk.

Neutral gas in shells has been seen as a problem for the phase-wrapping mechanism. Smoothed particle hydrodynamics modeling (Weil & Hernquist 1993) shows that gas-rich shells in radial orbits get easily stripped of their H I as shells cross paths. The main shell in NGC 3656 has apparently managed to keep some of its H I. Stripping efficiency may be reduced if the gas at the shell, and/or in the disk, is distributed in discrete clouds; the fate of gas in shells varies significantly depending on whether the gas is modeled as a continuous medium or as discrete clouds (Kojima & Noguchi 1997; Combes & Charmandaris 1999). The frequency of gas cloud collisions with the disk may be further reduced if the disk is geometrically thin.

5.2. *The Shell Unusual Brightness*

The southern shell of NGC 3656 is atypical for its high surface brightness (1.5 mag_R $arcsec^{-2}$ over the background; Fig. 2). Its integrated magnitude, after subtracting a smooth elliptical model of NGC 3656, is about $R = 15$, about 5% of the total R-band light of the galaxy. While its blue colors indicate young stars, the shell appears also in K-band images; hence, its high surface brightness cannot entirely be ascribed to young stellar populations. Taking into account $B-R \sim 1.0$ (B97), the shell has an absolute magnitude $M_B \sim 17$ comparable to that of a typical dwarf galaxy. This shell is thus produced by a fairly massive component. The pronounced surface brightness drop beyond the shell indicates that few stars at the shell location presently have orbital energies higher than those of the shell. Such order is hard to maintain after a pericenter passage near the galaxy center. These characteristics may probably be explained with a young age for the shell. The shell material still retains a memory of its initial orbit at present. Phase wrapping after several orbits might dilute the present shell into an ensemble of fainter shells with brightness comparable to those typically found in ellipticals.

With ~5% of the total galaxy light, presently the shell tidal field might influence the dynamics of the H I disk, perhaps contributing to its kinematic lopsidedness. N-body modeling should allow to test this hypothesis.

5.3. *Formation Scenarios*

NGC 3656 stands out among peculiar ellipticals for the number of features related to merger and accretion processes occurring simultaneously in the same object. What is the origin of so many peculiarities?

B97 proposes that NGC 3656 formed in a major merger of two spirals, given the presence of two optical tails. This merger should have formed the entire elliptical galaxy, including its system of shells, and have dumped the observed neutral gas. In merger simulations, the gaseous components of the precursor galaxies form centrally concentrated disks, while 5%–50% of the gas is ejected into extended tidal components (Barnes & Hernquist 1996; Barnes 2001), a picture that matches the H I distribution of NGC 3656. Spiral-spiral mergers produce polar gaseous rings under certain orbital configurations (Bekki 1998).

Shell formation in major mergers was modeled with N-body techniques by Hernquist & Spergel (1992). In their scenario, shells form out of returning tidal material. The fall-back of tidal material onto the merger remnant is beautifully portrayed for the prototype disk-disk merger NGC 7252 by Hibbard & Mihos (1995). In NGC 3656, that the

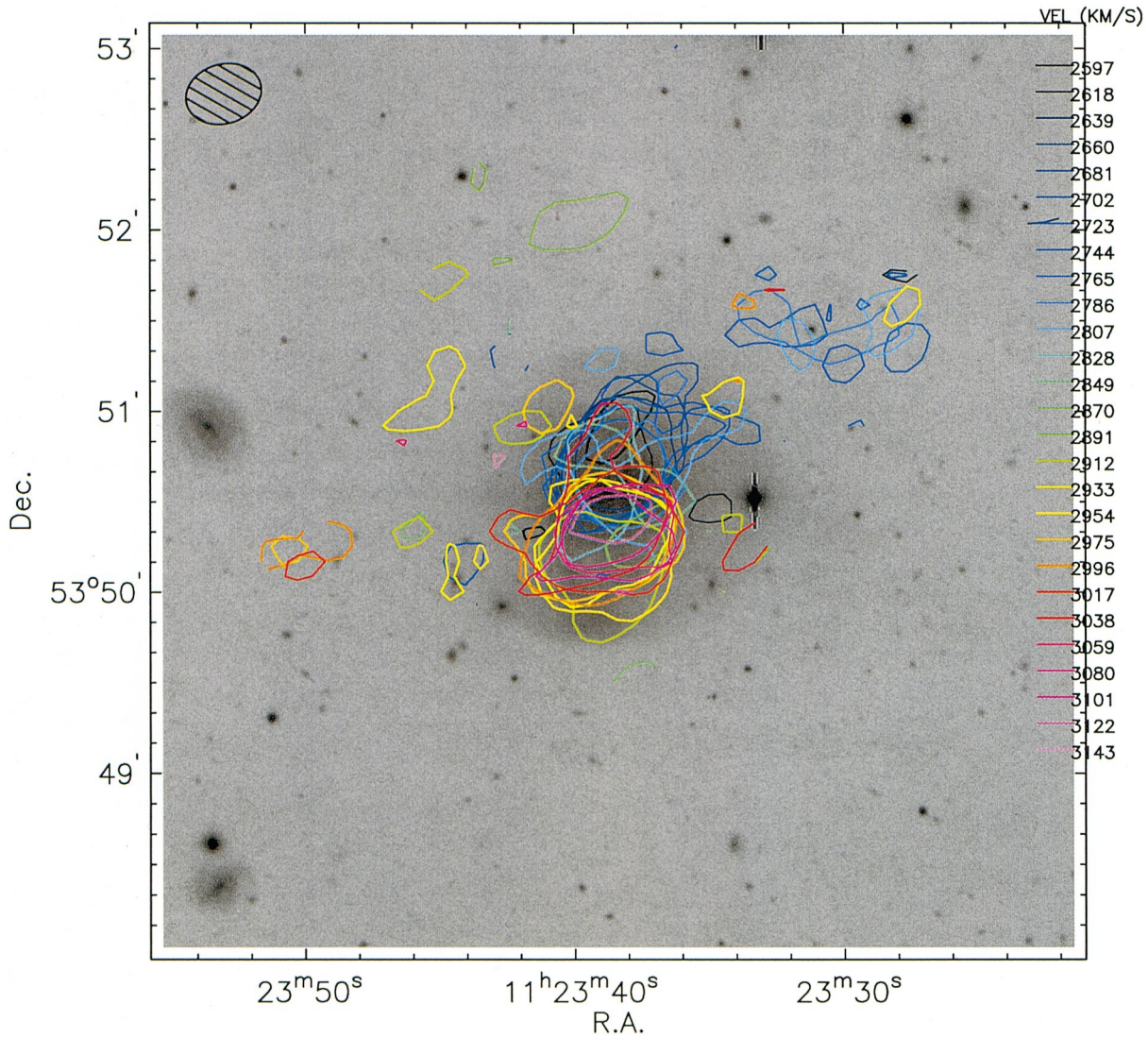

FIG. 7.—Contours of flux density 0.64 mJy beam^{-1} in the CD data cube, overlaid on an *R*-band image of NGC 3656. Velocities corresponding to each color are given in the legend. A mask was applied to each channel, built from a Gaussian-smoothed total H I map, in order to highlight the velocity structure of the extended components. Beam size is 25″.2 × 19″.7. Noise is 0.23 mJy beam^{-1} rms.

brightest shell lies at the base of one of the tidal tails and near the H I disk provides support for a connection of the shell to the gas accretion. That such a subsystem would have a sharp edge may be caused by the narrow ranges of orbital energy and angular momentum of the H I returning to the galaxy along the tidal tails. The blue colors in the shell also support the connection between the shell and the gas accretion. The lack of Hα significant emission, indicating the absence of early B-type stars, places a lower limit to the age of the shell stars at $\sim 10^7$ yr (e.g., Leitherer et al. 1999), while the presence of Hα in absorption places a less well defined upper limit at ~ 1.5 Gyr. The galaxy's crossing time at the shell radius is 0.6 Gyr. Hence, the spectral signatures at the shell indicate ages that are typical of advanced merger remnants, i.e., a few remnant's crossing times. Note that these ages are consistent with some of the stars being born in place after the accretion event, perhaps by compression of the gas clouds in their passage through the inner galaxy. The role of star formation in building shell systems has been largely unexplored and could be relevant to explaining the puzzling color properties of shells (Prieur 1990).

Overall, the major-merger hypothesis provides a consistent picture for the formation of the merger signatures of NGC 3656 in a single process. Other interpretations are also plausible, in which different processes account for the various peculiarities. The blue colors of the shell ($B-R \sim 1.0$; B97) correspond to those of a late-type, low-metallicity galaxy and thus could trace the ingestion of a satellite by NGC 3656. Several gas-rich galaxies exist in the vicinity of the galaxy, with sufficient gas to provide the $\sim 10^9\ M_\odot$ of H I present in the NGC 3656, while the accretion of other satellites could have produced the optical tidal tails and the shells. The presence of several gas-rich companions to H I–rich elliptical galaxies is common. For the NGC 3656 group to be bound, using the mass estimators of Heisler, Tremaine, & Bahcall (1985), we require from 3×10^{12} to $7.4 \times 10^{12}\ M_\odot$, yielding mass-to-light ratios $(M/L)_B$ from 125-300 in solar units (adding the light of all galaxies within 200 kpc and using our own photometry of NGC 3656, the dominant contributor). The halo mass is typical for L_* galaxies (Zaritsky et al. 1997), suggesting that the NGC 3656 group may indeed be bound. NGC 3656 may represent a case of a multiple accretion onto an exist-

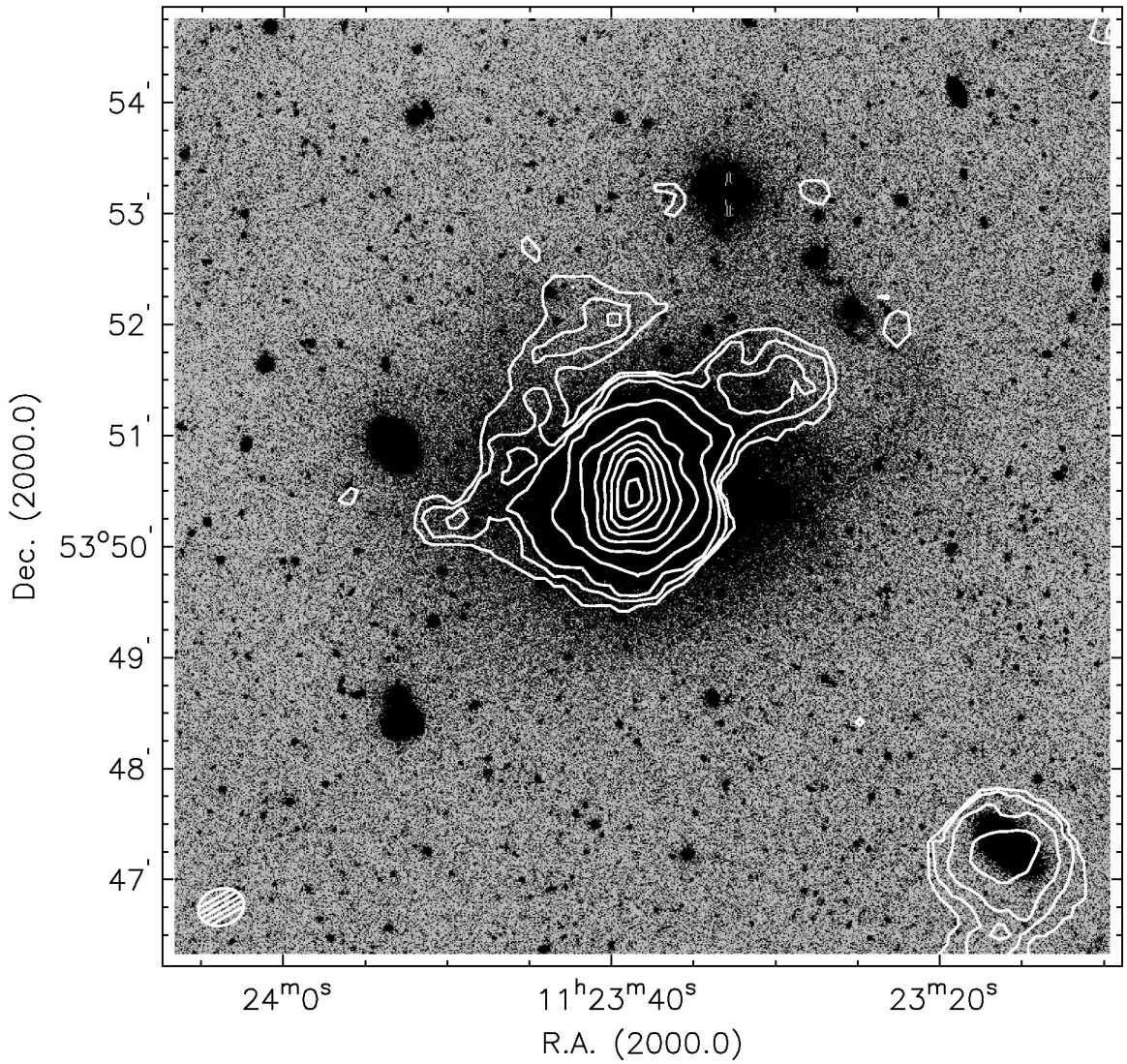

FIG. 8.—Contours of total H I flux from the CD array data. Beam is 25".2 × 19".7. H I contours are 0.23, 0.57, 1.1, 2.3, 4.6, 6.8, 9.1, 11.4, 13.7, and 16.0 × 10^{20} cm^{-2}. *Gray scale: R*-band image of NGC 3656, with gray scale stretched to show the faintest extended structures.

ing elliptical. Such process may continue in the future with the accretion of the five galaxies that lie within 180 kpc of NGC 3656, representing the collapse of a loose group leading to the formation of a massive field elliptical.

NGC 3656 shares striking similarities with the nearby elliptical NGC 5128, the parent galaxy to the radio source Cen A. B97 reviews the optical properties of these two galaxies, which have similar luminosities, effective radii, velocity dispersions, minor-axis dust disks, and systems of shells. The present paper shows that the similarities between these two galaxies extend to their distributions of H I, which both show a warped minor-axis rotating disk that extends outward to link with H I filaments aligned with the optical shells (Schiminovich et al. 1994; see also Sparke 1996). Evidence for star formation in the shells is given in NGC 3656 by the spectral (§ 2) and color (B97) signatures and in NGC 5128 by the detection of CO in the shells (Charmandaris, Combes, & van der Hulst 2000). These strong similarities might indicate that the type of merger and the nature of the progenitors is similar for these two galaxies, providing support for the hypothesis of a spiral-spiral merger for the formation of NGC 5128 (Schiminovich et al. 1994; Schweizer 1998).

NGC 3656 may be at an earlier stage in the merger evolution, as judged by the higher asymmetry of its optical image given by the prominent southern shell. Hence, we place NGC 3656 in an earlier stage than NGC 5128 in the merger age sequence of shell galaxies, and we note that the faint optical tails, H I complexes, and shell colors in NGC 3656 make a useful contribution toward filling the "King gap" (Toomre 1977) between merger remnants and normal ellipticals.

We thank Francoise Combes for her fast and constructive refereeing and M. Vogelaar for his assistance with the use of the GIPSY image processing system. This work has been supported in part by NSF grant AST 97-17177 to Columbia University. We acknowledge the use of NED and of the LEDA database.[8]

[8] Available at http://leda.univ-lyon1.fr.

REFERENCES

Arribas, S., et al. 1998, Proc. SPIE, 3355, 821
Balcells, M. 1997, ApJ, 486, L87 (B97)
Balcells, M., & Sancisi, R. 1996, AJ, 111, 1053 (BS96)
Balcells, M., & Stanford, S. A. 1990, ApJ, 362, 443 (BS90)
Barnes, J. E. 2001, in ASP Conf. Ser. 240, Gas and Galaxy Evolution, ed. J. E. Hibbard, M. P. Rupen, & J. H. van Gorkom (San Francisco: ASP), in press
Barnes, J. E., & Hernquist, L. 1996, ApJ, 471, 115
Bekki, K. 1998, ApJ, 499, 635
Charmandaris, V., Combes, F., & van der Hulst, J. M. 2000, A&A, 356, L1
Combes, F., & Charmandaris, V. 1999, in ASP Conf. Ser. 182, Galaxy Dynamics: A Rutgers Symposium, ed. D. Merritt, J. A. Sellwood, & M. Valluri (San Francisco: ASP), 489
del Burgo, C. 2000, Ph.D. thesis, Univ. La Laguna
Dupraz, C., & Combes, F. 1987, A&A, 185, L1
Heisler, J., Tremaine, S., & Bahcall, J. N. 1985, ApJ, 298, 8
Hernquist, L., & Quinn, P. J. 1987, ApJ, 312, 1
Hernquist, L., & Spergel, D. N. 1992, ApJ, 399, L117
Hibbard, J. E., & Mihos, J. C. 1995, AJ, 110, 140
Hibbard, J. E., Vacca, W. D., & Yun, M. S. 2000, AJ, 119, 1130
Hibbard, J. E., & van Gorkom, J. H. 1996, AJ, 111, 655
Hui, X., Ford, H. C., Freeman, K. C., & Dopita, M. 1995, ApJ, 449, 592
Jedrzejewski, R., & Schechter, P. L. 1988, ApJ, 330, L87
Kojima, M., & Noguchi, M. 1997, ApJ, 481, 132
Leitherer, C., et al. 1999, ApJS, 123, 3
Liu, C. T., & Kennicutt, R. C., Jr. 1995, ApJS, 100, 325
Mihos, J. C. 2001, ApJ, 550, 94
Möllenhoff, C., Hummel, E., & Bender, R. 1992, A&A, 255, 35
Prieur, J. L. 1990, in Dynamics and Interactions of Galaxies, ed. R. Wielen (Berlin: Springer), 72
Quinn, P. J. 1984, ApJ, 279, 596
Schiminovich, D., van Gorkom, J. H., & van der Hulst, J. M. 2001, AJ, submitted
Schiminovich, D., van Gorkom, J. H., van der Hulst, J. M., & Kasow, S. 1994, ApJ, 423, L101
Schiminovich, D., van Gorkom, J. H., van der Hulst, J. M., & Malin, D. F. 1995, ApJ, 444, L77
———. 1998, in Galaxies: Interactions and Induced Star Formation, ed. R. C. Kennicutt, Jr., et al. (Saas-Fee Advanced Course 26; Berlin: Swiss Soc. Astrophys. & Astron.), 105
———. 1996, ApJ, 473, 810
Toomre, A. 1977, in The Evolution of Galaxies and Stellar Populations, ed. B. M. Tinsley, R. B. Larson, & D. C. Gehret (New Haven: Yale Univ. Obs.), 401
van Gorkom, J. H., & Schiminovich, D. 1997, in ASP Conf. Ser. 116, Second Stromlo Symposium, The Nature of Elliptical Galaxies, ed. M. Arnaboldi, G. S. Da Costa, & P. Saha (San Francisco: ASP), 310
Weil, M. L., & Hernquist, L. 1993, ApJ, 405, 142
Zaritsky, D., Smith, R., Frenk, C., & White, S. D. M. 1997, ApJ, 478, 39

THE ASTRONOMICAL JOURNAL, 122:3508, 2001 December

ERRATUM: "H I IN THE SHELL ELLIPTICAL GALAXY NGC 3656" [ASTRON. J. **122**, 1758 (2001)]

MARC BALCELLS
Instituto de Astrofísica de Canarias

J. H. VAN GORKOM
Department of Astronomy, Columbia University

RENZO SANCISI
Osservatorio Astronomico di Bologna and Kapteyn Astronomical Institute

AND

CARLOS DEL BURGO
Instituto de Astrofísica de Canarias and Max-Planck-Institut für Astronomie
Received 2001 October 22; accepted 2001 October 24

As the result of an editorial oversight, the following two works were misattributed in the references:

Schweizer, F. 1998, in Galaxies: Interactions and Induced Star Formation, ed. D. Friedli, L. Martinet, & D. Pfenniger (Berlin: Springer), 105
Sparke, L. S. 1996, ApJ, 473, 810

The publisher regrets the error.